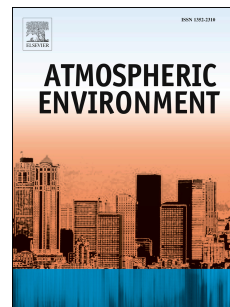# Accepted Manuscript

Effect of ambient humidity on the light absorption amplification of black carbon in Beijing during January 2013

Yunfei Wu, Renjian Zhang, Ping Tian, Jun Tao, S.-C. Hsu, Peng Yan, Qiyuan Wang, Junji Cao, Xiaoling Zhang, Xiangao Xia

Please cite this article as: Wu, Y., Zhang, R., Tian, P., Tao, J., Hsu, S.-C., Yan, P., Wang, Q., Cao, J., Zhang, X., Xia, X., Effect of ambient humidity on the light absorption amplification of black carbon in Beijing during January 2013, *Atmospheric Environment* (2015), doi: 10.1016/j.atmosenv.2015.04.041.

# Effect of ambient humidity on the light absorption amplification of black carbon in Beijing during January 2013

Yunfei Wu[1, *], Renjian Zhang[1, 2, *], Ping Tian[1, *], Jun Tao[3], S.-C. Hsu[4], Peng Yan[5], Qiyuan Wang[6], Junji Cao[6], Xiaoling Zhang[7] and Xiangao Xia[8]

[1]RCE-TEA, Institute of Atmospheric Physics, Chinese Academy of Sciences, Beijing 100029, China

[2]Collaborative Innovation Center on Forecast and Evaluation of Meteorological Disasters, Nanjing University of Information Science & Technology, Nanjing 210044, China

[3]South China Institute of Environmental Sciences, Ministry of Environmental Protection, Guangzhou 510655, China

[4]Research Center for Environmental Changes, Academia Sinica, Taipei, Taiwan

[5]CAWAS, Meteorological Observation Center of CMA, Beijing 100081, China

[6]Key Laboratory of Aerosol, SKLLQG, Institute of Earth Environment, Chinese Academy of Sciences, Xi'an 710075, China

[7]Institute of Urban Meteorology, Chinese Meteorological Administration, Beijing 100089, China

[8]LAGEO, Institute of Atmospheric Physics, Chinese Academy of Sciences, Beijing 100029, China

[*] These authors contributed equally to this work.

*Correspondence to:* Yunfei Wu (wuyf@mail.iap.ac.cn) and Renjian Zhang (zrj@mail.iap.ac.cn)

25 **Abstract**

26 Black carbon (BC) and its mixing state were measured with a ground-based single particle

27 soot photometer in urban Beijing during the extremely polluted winter of 2013. Up to $70 \pm$

28 $14\%$ of the BC-containing particles were thickly-coated during periods of haze, compared to

29 $37 \pm 9\%$ on non-hazy days. The thickly-coated number fraction ($NF_{BC-thick}$) increased with

30 increasing BC, reaching a plateau at ~80–90% when BC concentrations were $\geq 15$ µg m$^{-3}$ and

31 visibility was $\leq 2$ km. Regional inflows brought more aged, highly thickly-coated BC to

32 Beijing during haze. The absorption coefficient showed a distinct linear correlation with BC

33 concentration; the mass absorption efficiency (MAE) of BC was acquired, with an overall

34 mean of $4.2 \pm 0.01$ m$^2$ g$^{-1}$ at 870 nm. The MAE of BC amplified with increasing ambient

35 relative humidity. This was largely explained by the increase in $NF_{BC-thick}$, which was likely

36 due to the enhanced production of secondary aerosol under humid conditions.

37 **Keywords**: haze, black carbon, light absorption, ambient humidity

38

**1 Introduction**

Black carbon (BC), a highly condensed carbonaceous residue arising from incomplete combustion, is a major light-absorbing component in atmospheric aerosols. In addition to the impairment of visibility, BC also affects temperature, precipitation, and thus the climate of the Earth by altering the radiative balance of the atmosphere (Jacobson, 2001, 2002; Menon et al., 2002; Ramanathan and Carmichael, 2008). Globally, the positive direct radiative forcing induced by BC has been recently estimated at 1.1 W m$^{-2}$, larger than that of methane and is approximately two-thirds of that of carbon dioxide (Bond et al., 2013). Regional environments and climate are more sensitive to the effect of BC than carbon dioxide and methane, because of its shorter lifetime in the atmosphere (Ramanathan et al., 2007). Moreover, the adverse effects of BC particles on human health are also of great concern because they readily adsorb toxic substances as a result of their porous structure (Pope III and Dockery, 2006).

The annual BC emissions in China were estimated to have increased from 0.87 Tg in 1980 to 1.88 Tg in 2009, representing ~50% of the emissions in Asia and ~19% of global BC emissions (Qin and Xie, 2012). These substantial emissions have drawn great attention to the monitoring of BC concentrations in atmospheric aerosols across China (Cao et al., 2004, 2007; Y. F. Cheng et al., 2006; Zhang et al., 2009; T. T. Cheng et al., 2010; Zhuang et al., 2014b), as well as their related radiative forcing (Xia et al., 2007; Li et al., 2010; Zhuang et al., 2014a). However, the research into the sizes and mixing states of BC-containing particles, which have strong influence on the light absorption properties of BC, has been relatively scarce studied, mainly due to the limitations of the observational methodologies (Huang et al., 2011, 2012, 2013; Cheng et al., 2012; Wang et al., 2014). Laboratory experiments and theoretical computation have shown that thick coating by scattering components can enhance the absorption efficiency of typical BC particles in the ambient atmosphere by a factor of 1.5–2.0 (Schnaiter et al., 2005; Bond et al., 2006), which has been utilized in climate modeling (e.g., Chung et al., 2012). The mixing state of freshly emitted BC depends on combustion conditions. For instance, freshly emitted BC particles from vehicles are externally mixed,

67 subsequently being transformed into an internally mixed (coated) state through an aging

68 process associated with the condensation of reactive gases or coagulation with new

69 photochemically generated particles (Laborde et al., 2013 and references therein).

70 Haze, an 'atmospheric turbidity' phenomenon that arises due to a large amount of fine

71 particles suspended in the air through which visibility range is less than 10 km (Wu, 2011),

72 has become more frequent in China in recent years as a result of severe air pollution

73 combined with complex meteorological conditions (Zheng et al., 2015). The presence of haze

74 poses adverse effects on public health, regional climate, and, in turn, the economy. From

75 January to February 2013, East China, including Beijing, underwent a terrible heavily

76 polluted winter, with several consecutive and extensive air pollution events taking place,

77 leading to degraded visibility (Figure 1A). Studies have pointed out that fossil fuel

78 combustion is the most important source of fine particles suspended in the atmosphere over

79 China, especially during haze episodes (Zhang et al., 2013; Huang et al., 2014). As one of the

80 primary products from the combustion process and the dominant absorbing component, BC

81 plays an important and unique role in light extinction and radiative forcing. Although the BC

82 is lowly reactive in the atmosphere, the stable synoptic meteorological condition and high

83 ambient relative humidity during haze episodes favors the formation of secondary aerosols

84 (Sun et al., 2013; Zheng et al., 2015), which have a potential impact on the properties of

85 BC-containing particles. In this study, we investigate the characteristics of BC-containing

86 particles and examine how the absorption properties vary in response to their different

87 characteristics, particularly in terms of internal mixing state, and meteorological conditions

88 during the extreme pollution period.

89 **2 Methodology**

90 BC measurements were conducted using a single particle soot photometer (SP2, Droplet

91 Measurement Technologies, Inc.) from 9 to 27 January 2013 on the rooftop (approximately 8

92 m above ground level) of an experimental building at the Tower Division of the Institute of

93 Atmospheric Physics, Chinese Academy of Sciences, which lies between the North 3rd and 4th

94 Ring Road of Beijing (39º 58' N, 116º 22' E). This observation site is a typical urban site

95    surrounded by residential areas and is located near a busy highway. Combustion and traffic

96    emissions are the major local sources of air pollutants.

97    The SP2 has been widely adopted in studies of the characteristics of BC because of its high

98    resolution and accuracy. The SP2 measures BC mass in individual particles according to the

99    intensity of incandescent light, which is independent of the BC-containing particle

100   morphology or mixing state (Slowik et al., 2007). For further details on the operating

101   principles of SP2 see Schwarz et al. (2006). In this campaign, the SP2 was operated at a

102   relatively low flow rate (30 cc/min) to reduce the multi-particle coincidence issues that occur

103   under heavy pollution. Generally, the SP2 detects BC core sizes in the range of 0.07–0.5 μm

104   in mass equivalent diameter, assuming a void-free material density of 1.8 g cm$^{-3}$. A sharp

105   falloff in SP2 detection efficiency has been observed at smaller BC core sizes (e.g., <1 fg or

106   100 nm in mass equivalent diameter reported by Laborde et al. 2012b). The incandescence

107   signals are usually saturated in the case of particles with a BC core size larger than 500 nm,

108   leading to an underestimation of the BC masses. Therefore, a lognormal fit to the BC mass

109   size distribution in the range of <1 μm was performed once per hour to make up the missing

110   BC masses below 100 nm and larger than 500 nm. The incandescence signal was calibrated

111   pre-, mid- and post-sampling using the generated standard soot particles (classic Aquadag) in

112   the size range of 100–350 nm in mobility diameter, selected by a differential mobility

113   analyzer. Linear calibration curves between the incandescence signals and the masses of

114   size-selected soot particles were extracted, and were shown to be stable during the campaign

115   (Figure S1). It is notable that recent studies have shown that Aquadag soot is more sensitive

116   to the incandescence signals and results in an underestimation of ~25% of the measured BC

117   masses (Laborde et al., 2012a). Thus, the BC masses directly determined according to the

118   calibration with Aquadag soot were divided by a factor of 0.75 before the following analysis

119   in this study. The uncertainty in BC masses determined by SP2 was ~25%, including the

120   uncertainties inherent in mass calibration, flow measurement and the estimation of BC masses

121   beyond the SP2 detection range (Schwarz et al., 2008; Wang et al., 2014).. Monodisperse

122   polystyrene latex spheres (PSL) with a diameter of 269 nm were generated daily and

123   delivered to the SP2 to check the laser intensity and instrument stability throughout the

124   experiment. A decrease by ~30% in the peak of scattering signal was found, suggesting

125 caution in the use of our SP2's scattering signals (Figure S2). However, the decrease did not

126 influence the BC mass measurements significantly, as the three BC calibrations agreed

127 consistently with each other throughout the campaign (Figure S1). Thus, the time-lag method,

128 which is applicable regardless of the intensity of scattering signal, was utilized in this study to

129 identify the mixing state of BC-containing particles. Based on the minimum in the bimodal

130 frequency distribution of delay times between the peaks of the incandescence and scattering

131 signal (Moteki et al., 2007), a single BC-containing particle with a time lag greater than 2 μs

132 was recognized as being thickly-coated (BC thickly coated by other matters) (Figure S3).

133 A photoacoustic extinctiometer (PAX, Droplet Measurement Technologies, Inc.) was set

134 behind a silica gel diffuse dryer to measure the dry aerosol absorption coefficient ($\sigma_{abs}$) every

135 10 seconds based on photoacoustic theories, as described by Arnott et al. (1999). The

136 wavelength of the PAX employed is 870 nm. Calibration was carried out prior to observation

137 using pure scattering particles (ammonium sulfate) and soot particles (classic Aquadag) at

138 high concentrations, following the procedure suggested by the manufacturer, which is also

139 generally described in Wang et al. (2014). Only the particulate matter with a size less than 2.5

140 μm in aerodynamic diameter ($PM_{2.5}$) was measured, by setting the inlets of the SP2 and PAX

141 with $PM_{2.5}$ cutoffs.

142 Visibility was detected using a visibility sensor (Model 6000, Belfort) set alongside the

143 experimental room. A high output infrared LED transmitter projects light into a sample

144 volume and light scattered in a forward direction (42º) is collected by the receiver. The light

145 source is modulated to provide excellent rejection of background noise and natural variations

146 in background light intensity. The sensor's analog output signal is proportional to visibility.

147 Meteorological parameters including relative humidity (RH), wind velocity and direction

148 were obtained from a 325 m tower located approximately 50 m north of our observation site.

149 The parameters recorded at 47 m height were utilized in this study. All the mentioned data

150 were averaged by 5-min for the following analysis. The hourly $PM_{2.5}$ mass concentrations

151 used were monitored at another urban Beijing site, Baolian, by the Institute of Urban

152 Meteorology (Zhao et al., 2009), which is located less than 10 km away from our site.

153    **3 Results and Discussion**

154    **3.1 Visibility degradation and PM$_{2.5}$ and BC increase**

155    Beijing experienced 14 haze days during the 19 day observation period, including four severe

156    haze events with a visibility of less than 2 km, one of which an continued for a total 64 hours,

157    extending from 09:00 AM on 12 January to 01:00 AM on 15 January 2013 (Figure 1A).

158    During the haze events, visibility degradation corresponded to the increase in PM$_{2.5}$ and BC

159    mass concentrations (Figure 1B). PM$_{2.5}$ and BC concentrations varied synchronously, with a

160    correlation coefficient of R = 0.88 (n = 375, p < 0.001); the maximum hourly concentrations

161    were up to 632 µg m$^{-3}$ for PM$_{2.5}$ and 25.3 µg m$^{-3}$ for BC. On average, BC constituted 5.7% of

162    PM$_{2.5}$, which is comparable to the filter-based fractions observed in Beijing, with a value of

163    4.5% during the winter of 2010 (Zhang et al., 2013) and 3.5% in January of 2013 (Huang et

164    al., 2014). Notably, BC mass fraction in PM$_{2.5}$ varied from 4.0% when heavy haze was

165    present (visibility < 2 km) to 7.4% when haze was absent (Table 1), indicating aerosol

166    components other than BC increased more during haze events. From the real-time

167    measurements of aerosol chemical compositions during a similar period (1–16 January 2013),

168    Sun et al. (2014) found that the role of secondary inorganic species was enhanced during the

169    formation of the haze events. Using filter-based analysis, Huang et al. (2014) also showed that

170    the severe haze was to a large extent driven by secondary aerosol formation. The BC

171    concentration, with the mean of 5.5 µg m$^{-3}$, is very close to the values reported by Huang et al.

172    (2014) and Zhang et al. (2015) despite utilization of completely different methodologies

173    (Table S1). Meanwhile, the BC concentration in this study is not considerably higher and

174    even lower than those previously measured in urban Beijing during wintertime (Table S1);

175    even the haze events were reported to be severely and frequently during January 2013 (Zheng

176    et al., 2015). In summary, BC fractions (in unit %) decreased during the heavily polluted

177    PM$_{2.5}$ episodes in Beijing, though its atmospheric concentrations (in µg m$^{-3}$) increased.

178    Compared to the measurements produced using SP2 over China in wintertime, the mean BC

179    concentration in this study is moderate. The mean BC concentrations at urban sites were 8.8

180    µg m$^{-3}$ in Xi'an (Wang et al., 2014), 7.1 µg m$^{-3}$ in Shanghai (Huang et al., 2013) and 4.1 µg

181 m$^{-3}$ in Shenzhen (Huang et al., 2012). As summarized in Table S2, the annual BC emission in

182 Beijing is 15.75 Gg in 2009, of which 4.70 Gg (~30%) was contributed by transportation (Qin

183 and Xie, 2012). When compared to Guangdong (i.e., the Pearl River Delta region), the total

184 BC emission and the contribution from transportation are much smaller in Beijing, but similar

185 in magnitude to Shanghai (Table S2). Sources other than transportation contributed the greater

186 part of BC in Beijing.

187 **3.2 Absorption properties**

188 Figure 1C shows the time-series of $\sigma_{abs}$ at 870 nm, in addition to the number fraction of

189 thickly-coated BC (NF$_{BC\text{-}thick}$), which was defined as the ratio of the number concentration of

190 thickly-coated BC-containing particles to that of overall BC-containing particles, measured

191 during this campaign. The 870 nm $\sigma_{abs}$ varied from 0.4 to 114.2 Mm$^{-1}$, and had an average of

192 33.1 Mm$^{-1}$ during the haze events and only 8.2 Mm$^{-1}$ during the non-haze periods (Table 1).

193 In addition, it is clear that its variation also worked in concert with visibility, PM$_{2.5}$, and BC

194 (Figures 1A and 1B). The overall mean $\sigma_{abs}$ (23.6 Mm$^{-1}$ at 870 nm) in this study is slightly

195 higher than that measured during summer at a rural site in the Pearl River Delta region (~21.0

196 Mm$^{-1}$) (Garland et al., 2008) and in urban Shenzhen (~15.8 Mm$^{-1}$) (Lan et al., 2013) during

197 summer, but is much lower than that in urban Guangzhou in autumn (~56.5 Mm$^{-1}$ at 870 nm)

198 (Andreae et al., 2008). Note that an assumption of the inverse wavelength "Power-law" (i.e.,

199 $\sigma_{abs1}/\sigma_{abs2} = \lambda_2/\lambda_1$) was made to convert the $\sigma_{abs}$ at other wavelengths to that at 870 nm.

200 Light absorption at 870 nm is dominated by BC, which is revealed by the high correlation (R$^2$

201 = 0.97) and low y-intercept value (~0.4 Mm$^{-1}$) of the linear regression of $\sigma_{abs}$ against BC

202 concentration (Figure 2A). The slope of the regression line represents the bulk mass

203 absorption efficiency of BC, an important optical property of BC (i.e., MAE = $\sigma_{abs}$ / BC mass

204 concentration). The resulting bulk MAE at 870 nm is 4.2 ± 0.01 m$^2$ g$^{-1}$, whereas it appeared to

205 vary with ambient RH (Figure 2A). It does not obviously deviate from the central estimate

206 (~7.5 m$^2$ g$^{-1}$ at 550 nm, equivalent to ~4.7 m$^2$ g$^{-1}$ at 870 nm) of ambient BC particles

207 presented by Bond and Bergstrom (2006). Although based on similar methods, the mean

208 MAE in our study is much lower than that acquired in another urban site in China, Xi'an (7.6

8

209
210
211

$\pm$ 0.02 m$^2$ g$^{-1}$ at 870 nm, Wang et al., 2014), while it is comparable to Shengzhen (6.5 m$^2$ g$^{-1}$ at 532 nm, equivalent to ~4.0 m$^2$ g$^{-1}$ at 870 nm, Lan et al., 2013). This suggests that there are large spatial and temporal disparities in the absorption ability of BC.

212     **3.3 Mixing state of BC**

213     In this campaign, thickly-coated BC-containing particles constituted a significant fraction,

214     with NF$_{BC-thick}$ of up to 70% in the hazy periods compared to only 37% during the non-haze

215     periods (Table 1). Overall, there was a positive correlation between NF$_{BC-thick}$ and BC

216     concentration, with an increasing trend reached saturation point at NF$_{BC-thick}$ = ~80–90% when

217     BC concentrations were ~15 µg m$^{-3}$ or larger and visibility was always less than 2 km (Figure

218     2B). However, the relationship varied in response to pollution extent. As presented in Figure

219     2B and Table S3, a negative correlation between NF$_{BC-thick}$ and BC concentration was

220     observed during the non-haze periods (visibility > 10 km). However, in the haze periods

221     (visibility < 10 km), NF$_{BC-thick}$ increased with increasing BC concentration. The negative

222     correlation during clean periods can be explained by the diurnal variations of NF$_{BC-thick}$ and

223     BC concentration. Usually, BC concentration is higher in the morning when more freshly (i.e.,

224     non/thinly-coated) BC particles are emitted from vehicle exhaust, whereas it is lower in the

225     afternoon because of the elevation of mixing layer height concurrently with the formation of

226     more thickly-coated BC particles due to the increasing production of secondary aerosols

227     (Figure S4). The increasing thickly-coated state of BC aerosols during haze periods arises

228     from the combined effect of aging processes from involvement in heterogeneous reactions

229     en-route, in addition to the increasing production of secondary aerosol under stable weather

230     conditions (Sun et al., 2013; Zheng et al., 2015).. Based on potential source contribution

231     function analysis, Zhang et al. (2013) determined that trans-boundary transport from

232     surrounding areas/cities is a major contributor of BC in Beijing. In the present study, we

233     found that elevated BC and thickly-coated mixing state was closely associated with either

234     weak winds (wind speed < 2 m s$^{-1}$) or stronger southeasterly winds (wind speed ~4 m s$^{-1}$)

235     (Figure S5). Of these, the former was favorable for pollutant buildup regardless of local and

236     long-range transported sources, and the latter brought the highly polluted airs from the

237  provinces of Tianjing, Liaoning, and Hebei, which are all well known heavy industrial areas

238  (Jung *et al* 2009).

239  Typical urban BC emissions were characterized by much less coating (only 9%) than biomass

240  burning (up to 70%) (Schwarz et al., 2008). Fine sized sulfate and organics, which are

241  prevalent in China, accounted for the coatings of BC measured downstream of China's

242  pollution outflows (Shiraiwa et al., 2007). Accordingly, the increase in $NF_{BC\text{-thick}}$ during the

243  haze events revealed that the highly internally-mixed (i.e., thickly-coated) BC aerosols were

244  mostly originated from regionally transported, aged BC, instead of local sources. This

245  suggestion agrees with the results of Sun et al. (2014), showing that more than half of

246  pollutants during haze periods in Beijing can be attributed to regional transport.

247  **3.4 Ambient humidity effect on light absorption**

248  Interestingly, as shown in Figure 2A, the MAE of BC appeared to vary with the ambient RH.

249  The relationship was further investigated by comparing the MAE with ambient RH directly.

250  Before that, the BC concentration was previously divided into three levels according to its

251  percentile, with the BC concentration in the range of 25–50$^{th}$ percentile as the slightly

252  polluted case, 50–75$^{th}$ as the moderately polluted, and >75$^{th}$ percentile as the heavily polluted.

253  The comparison was independently performed at each pollution level to reduce the impact of

254  BC concentration on the MAE. Note that the case with BC concentration <25$^{th}$ percentile was

255  not presented because of the few samples at high RH during the clean periods. Positive

256  correlations between the MAE and ambient RH are observed, with correlation coefficients of

257  0.32 (n = 1199, p < 0.001), 0.41 (n = 1218, p < 0.001) and 0.59 (n = 1227, p < 0.001),

258  respectively in the slightly, moderately and heavily polluted case.. Plotting the mean MAE

259  against the increasing ambient RH bins (bin width = 10%) shows the amplification of MAE

260  more clearly, especially in the more polluted cases (Figure 3A). As the ambient RH increases

261  from 40–50% to 80–90%, the mean MAE enhances from 4.1 to 5.0 m$^2$ g$^{-1}$ (by ~22%) in the

262  moderately polluted case, and 3.8 to 4.7 m$^2$ g$^{-1}$ (by ~24%) in the heavily polluted case. The

263  increases are statistic significant at 99.9% confidence level using the student's *t*-test. Simply

264  applying the linear regression of MAE against the ambient RH, the rates of increase are

10

265 estimated to be 0.20 and 0.24 $m^2 g^{-1}$/10% RH, respectively in the moderately and heavily

266 polluted case.. The increase in MAE can be largely explained by the increase in $NF_{BC-thick}$ in

267 response to the increasing ambient RH. As shown in Figure 3B, the corresponding increases

268 in the mean $NF_{BC-thick}$ are from 58 to 78% (by ~34%) and 71 to 84% (by ~18%) in the two

269 polluted cases, respectively. Thickly coating by scattering components can enhance the MAE

270 of typical BC particles in ambient atmosphere by a factor of 1.5–2.0 (Schnaiter et al., 2005;

271 Bond et al., 2006). In-situ measurement has shown that the production of sulfate and coal

272 combustion organic aerosol increased greatly with increasing RH during the wintertime in

273 Beijing (Sun et al., 2013). At a certain BC concentration level, the increase in the production

274 of secondary aerosol (e.g., sulfate and organic aerosol) with increasing ambient RH will

275 increase the probability of BC particles becoming thickly-coated by these secondary

276 components through the aqueous-phase reaction, resulting in the amplification of MAE.

277 It is notable that the increase of MAE in the slightly polluted case appears to stagnate and

278 even reverse when ambient RH is greater than 60%, despite the $NF_{BC-thick}$ gradually increases

279 with increasing RH (Figure 3). Moreover, although the increase in MAE with increasing

280 ambient RH can be largely explained by the increasing coating of BC particles in each BC bin,

281 the relationship between MAE and $NF_{BC-thick}$ among the different BC pollution levels is

282 ambiguous. The $NF_{BC-thick}$ was generally higher in the heavily polluted case; however, the

283 MAE was even lower when compared to those in the slightly and moderately polluted cases.

284 In addition to the thickness and chemical/optical properties of the coating materials, particle

285 sizes are also likely to have a considerable impact on the absorption efficiency of

286 BC-containing particles. The MAE of BC decreases significantly once when the BC size is

287 larger than ~150 nm in diameter (Figure 4 in Bond and Bergstrom, 2006). The amplification

288 of MAE with the increasing $NF_{BC-thick}$ might be suppressed by the increase in the BC sizes.

289 However, this is beyond the scope of this study and would require further investigation of the

290 aerosol sizes and chemical components.


291 **3.5 Summary and concluding remarks**


292 In this study, the BC absorption and mixing state during extremely polluted wintertime haze

293  events in Beijing were investigated using the advanced SP2. In January 2013, when hourly

294  $PM_{2.5}$ concentrations reached an extreme of ~632 µg m$^{-3}$ in Beijing, mass concentrations and

295  absorption coefficients of BC were simultaneously measured. The results were subject to

296  interpretation in conjunction with various other measurements, particularly with respect to the

297  effect of ambient RH on absorption amplification of BC aerosols. Large discrepancies in BC

298  concentration and $NF_{BC\text{-}thick}$ were found between the hazy and non-hazy periods, i.e., $7.6 \pm 4.8$

299  versus $2.0 \pm 1.2$ µg m$^{-3}$, and $70 \pm 14\%$ versus $37 \pm 9\%$, respectively, which accounted for the

300  observed significant difference in $\sigma_{abs}$ (at 870 nm) between the two periods, i.e., $33.1 \pm 20.2$

301  versus $8.2 \pm 5.2$ Mm$^{-1}$. Generally, the $NF_{BC\text{-}thick}$ increased with increasing BC concentration

302  and decreasing visibility. It remained at a nearly constant $NF_{BC\text{-}thick}$ of ~80–90% when BC

303  concentration approached 15 µg m$^{-3}$ or higher. A distinct linear correlation between $\sigma_{abs}$ and

304  the BC concentration was shown. Thus, the bulk MAE of BC (at 870 nm) was estimated,

305  averaging $4.2 \pm 0.01$ m$^2$ g$^{-1}$ while varying with ambient RH. The MAE of BC was amplified

306  as the ambient RH increased which was largely explained by the increase in $NF_{BC\text{-}thick}$. This

307  increase was most likely due to the enhanced production of secondary aerosol under humid

308  conditions during the cold wintertime.

309  Through the analysis in the study, the highly thickly-coated BC was considered to be

310  dominated by regionally transported aged BC from heavily polluted areas that surround

311  Beijing. This also corresponded to the finding that the BC mass fraction in $PM_{2.5}$ was smaller

312  during the hazy periods (5.2%) than during the non-haze periods (7.4%), when local pollution

313  dominated. This result further implies that better understanding of $PM_{2.5}$ composition is

314  necessary to explicitly study the optical effect of various chemical mixtures of BC aerosols.

315  The results of our study could facilitate atmospheric chemistry and climate modeling on

316  regional/global scales in terms of the direct forcing of BC and its influencing factors. They

317  may also shed light on the implementation of air quality management and BC emissions

318  control in Beijing.

324

325  **References**

326  Andreae, M.O., Schmid, O., Yang, H., Chand, D., Yu, J.Z., Zeng, L.M., Zhang, Y.H., 2008.

327      Optical properties and chemical composition of the atmospheric aerosol in urban

328      Guangzhou,        China.        Atmos.        Environ.        42,        6335–6350.

329      http://dx.doi.org/10.1016/j.atmosenv.2008.01.030.

330  Arnott, W.P., Moosmüller, H., Rogers, C.F., Jin, T.F., Bruch, R., 1999. Photoacoustic

331      spectrometer for measuring light absorption by aerosol: instrument description. Atmos.

332      Environ. 33, 2845–2852.

333  Bond, T.C., Bergstrom, R.W., 2006. Light absorption by carbonaceous particles: An

334      investigative        review.        Aerosol        Sci.        Technol.        40,        27–67.

335      http://dx.doi.org/10.1080/02786820500421521.

336  Bond, T.C., Habib, G. Bergstrom, R.W., 2006. Limitations in the enhancement of visible light

337      absorption        due        to        mixing        state.        J.        Geophys.        Res.        111,        D20211.

338      http://dx.doi.org/10.1029/2006JD007315.

339  Bond, T.C., et al., 2013. Bounding the role of black carbon in the climate system: A scientific

340      assessment.    J. Geophys. Res. 118, 5380–5552. http://dx.doi.org/10.1002/jgrd.50171.

341  Cao, J.J., Lee, S.C., Ho, K.F., Zou, S.C., Fung, K., Li, Y., Watson, J.G., Chow, J.C., 2004.

342      Spatial and seasonal variations of atmospheric organic carbon and elemental carbon in

343      Pearl    River    Delta    Region,    China.    Atmos.    Environ.    38,    4447–4456.

344      http://dx.doi.org/10.1016/j.atmosenv.2004.05.016.

345  Cao, J.J., Lee, S.C., Chow, J.C., Watson, J.G., Ho, K.F., Zhang, R.J., Jin, Z.D., Shen, Z.X.,

346      Chen, G.C., Kang, Y.M., Zou, S.C., Zhang, L.Z., Qi, S.H., Dai, M.H., Cheng, Y., Hu, K.,

347      2007. Spatial and seasonal distributions of carbonaceous aerosols over China. J.

348      Geophys. Res. 112, D22S11. http://dx.doi.org/10.1029/2006JD008205.

349    Cheng, T.T., Han, Z.W., Zhang, R.J., Du, H.H., Jia, X., Wang, J.J., Yao, J.Y., 2010. Black

350         carbon in a continental semi-arid area of Northeast China and its possible sources of fire

351         emission. J. Geophys. Res. 115, D23204. http://dx.doi.org/10.1029/2009JD013523.

352    Cheng, Y.F., Lee, S.C., Ho, K.F., Wang, Y.Q., Cao, J.J., Chow, J.C., Watson, J.G., 2006. Black

353         carbon measurement in a coastal area of south China. J. Geophys. Res. 111, D12310.

354         http://dx.doi.org/10.1029/2005JD006663.

355    Cheng, Y.F., Su, H., Rose, D., Gunthe, S.S., Berghof, M., Wehner, B., Achtert, P., Nowak, A.,

356         Takegawa, N., Kondo, Y., Shiraiwa, M., Gong, Y.G., Shao, M., Hu, M., Zhu, T., Zhang,

357         Y.H., Carmichael, G.R., Wiedensohler, A., Andreae, M.O., Pöschl, U., 2012.

358         Size-resolved measurement of the mixing state of soot in the megacity Beijing, China:

359         diurnal cycle, aging and parametrization. Atmos. Chem. Phys. 12, 4477–4491.

360         http://dx.doi.org/10.5194/acp-12-4477-2012.

361    Chung, C.E., Lee, K., Muller, D., 2012. Effect of internal mixture on black carbon radiative

362         forcing. Tellus B 64, 10925. http://dx.doi.org/10.3402/tellusb.v64i0.10925.

363    Garland, R.M., Yang, H., Schmid, O., Rose, D., Nowak, A., Achtert, P., Wiedensohler, A.,

364         Takegawa, N., Kita, K., Miyazaki, Y., Kondo, Y., Hu, M., Shao, M., Zeng, L.M., Zhang,

365         Y.H., Andreae, M.O., Pöschl, U., 2008. Aerosol optical properties in a rural environment

366         near the mega-city Guangzhou, China: implications for regional air pollution, radiative

367         forcing and remote sensing. Atmos. Chem. Phys. 8, 5161–5186. http://dx.doi.org/

368         10.5194/acp-8-5161-2008.

369    Huang, X.F., Gao, R.S., Schwarz, J.P., He, L.Y., Fahey, D.W., Watts, L.A., McComiskey, A.,

370         Cooper, O.R., Sun, T.L., 2011. Black carbon measurements in the Pearl River Delta

371         region    of    China.    J.    Geophys.    Res.    116,    D12208.

372         http://dx.doi.org/10.1029/2010JD014933.

373    Huang, X.F., Sun, T.L., Zeng, L.W., Yu, G.H., Luan, S.J., 2012. Black carbon aerosol

374         characterization in a coastal city in South China using a single particle soot photometer.

375         Atmos. Environ. 51, 21–28. http://dx.doi.org/10.1016/j.atmosenv.2012.01.056.

376    Huang, X.F., Xue, L., Tian, X.D., Shao, W.W., Sun, T.L., Gong, Z.H., Ju, W.W., Jiang, B., Hu,

377         M., He, L.Y., 2013. Highly time-resolved carbonaceous aerosol characterization in

378         Yangtze River Delta of China: Composition, mixing state and secondary formation.

14

379    Atmos. Environ. 64, 200–207. http://dx.doi.org/10.1016/j.atmosenv.2012.09.059.

380  Huang, R.J., et al., 2014. High secondary aerosol contribution to particulate pollution during

381    haze events in China. Nature 514, 218–222. http://dx.doi.org/10.1038/nature13774.

382  Jacobson, M.Z., 2001. Strong radiative heating due to the mixing state of black carbon in

383    atmospheric aerosols. Nature 409, 695–697. http://dx.doi.org/10.1038/35055518.

384  Jacobson, M.Z., 2002. Control of fossil-fuel particulate black carbon and organic matter,

385    possibly the most effective method of slowing global warming. J. Geophys. Res.

386    107(D19), 4410. http://dx.doi.org/10.1029/2001JD001376.

387  Jung, J.S., Lee, H.L., Kim, Y.J., Liu, X.G., Zhang, Y.H., Hu, M., Sugimoto, N., 2009. Optical

388    properties of atmospheric aerosols obtained by in situ and remote measurements during

389    2006 Campaign of Air Quality Research in Beijing (CAREBeijing-2006). J. Geophys.

390    Res. 114, D00G02. http://dx.doi.org/10.1029/2008JD010337.

391  Laborde, M., Mertes, P., Zieger, P., Dommen, J., Baltensperger, U., Gysel, M., 2012a.

392    Sensitivity of the Single Particle Soot Photometer to different black carbon types. Atmos.

393    Meas. Tech. 5, 1031–1043. http://dx.doi.org/10.5194/amt-5-1031-2012.

394  Laborde, M., Schnaiter, M., Linke, C., Saathoff, H., Naumann, K.H., Möhler, O., Berlenz, S.,

395    Wagner, U., Taylor, J.W., Liu, D., Flynn, M., Allan, J.D., Coe, H., Heimerl, K.,

396    Dahlkötter, F., Weinzierl, B., Wollny, A.G., Zanatta, M., Cozic, J., Laj, P., Hitzenberger,

397    R., Schwarz, J.P., Gysel, M., 2012b. Single Particle Soot Photometer intercomparison at

398    the    AIDA    chamber.    Atmos.    Meas.    Tech.    5,    3077–3097.

399    http://dx.doi.org/10.5194/amt-5-3077-2012.

400  Laborde, M., Crippa, M., Tritscher, T., Jurányi, Z., Decarlo, P.F., Temime-Roussel, B.,

401    Marchand, N., Eckhardt, S., Stohl, A., Baltensperger, U., Prévôt, A.S.H., Weingartner, E.,

402    Gysel, M., 2013. Black carbon physical properties and mixing state in the European

403    megacity    Paris.    Atmos.    Chem.    Phys.    13,    5831–5856.

404    http://dx.doi.org/10.5194/acp-13-5831-2013.

405  Lan, Z.J., Huang, X.F., Yu, K.Y., Sun, T.L., Zeng, L.W., Hu, M., 2013. Light absorption of

406    black carbon aerosol and its enhancement by mixing state in an urban atmosphere in

407    South    China.    Atmos.    Environ.    69,    118–123.

408    http://dx.doi.org/10.1016/j.atmosenv.2012.12.009.

409    Li, Z.Q., Lee, K.H., Wang, Y.S., Xin, J.Y., Hao, W.M., 2010. First observation-based

410        estimates of cloud-free aerosol radiative forcing across China. J. Geophys. Res. 115,

411        D00K18. http://dx.doi.org/10.1029/2009JD013306.

412    Menon, S., Hansen, J., Nazarenko, L., Luo, Y.F., 2002. Climate effects of black carbon

413        aerosols    in    China    and    India.    Science    297,    2250–2253.

414        http://dx.doi.org/10.1126/science.1075159.

415    Moteki, N., Kondo, Y., Miyazaki, Y., Takegawa, N., Komazaki, Y., Kurata, G., Shirai, T.,

416        Blake, D.R., Miyakawa, T., Koike, M., 2007. Evolution of mixing state of black carbon

417        particles: aircraft measurements over the Western Pacific in March 2004. Geophys. Res.

418        Lett. 34, L11803. http://dx.doi.org/10.1029/2006GL028943.

419    Pope III, C.A., Dockery, D.W., 2006. Critical review: health effects of fine particulate air

420        pollution: Lines that connect. J. Air Waste Manage. 56, 709–742.

421    Qin, Y., Xie, S.D., 2012. Spatial and temporal variation of anthropogenic black carbon

422        emissions in China for the period 1980-2009. Atmos. Chem. Phys. 12, 4825–4841.

423        http://dx.doi.org/10.5194/acp-12-4825-2012.

424    Ramanathan, V., Li, F., Ramana, M.V., Praveen, P.S., Kim, D., Corrigan, C.E., Nguyen, H.,

425        Stone, E.A., Schauer, J.J., Carmichael, G.R., Adhikary, B., Yoon, S.C., 2007.

426        Atmospheric brown clouds: Hemispherical and regional variations in long-range

427        transport, absorption, and radiative forcing. J. Geophys. Res. 112, D22S21.

428        http://dx.doi.org/ 10.1029/2006JD008124.

429    Ramanathan, V., Carmichael, G., 2008. Global and regional climate changes due to black

430        carbon. Nature Geoscience 1, 221–227. http://dx.doi.org/10.1038/ngeo156.

431    Schnaiter, M., Linke, C., Möhler, O., Naumann, K.H., Saathoff, H., Wagner, R., Schurath, U.,

432        Wehner, B., 2005. Absorption amplification of black carbon internally mixed with

433        secondary    organic    aerosol.    J.    Geophys.    Res.    110,    D19204.

434        http://dx.doi.org/10.1029/2005JD006046.

435    Schwarz, J.P., Gao, R.S., Fahey, D.W., Thomson, D.S., Watts, L.A., Wilson, J.C., Reeves,

436        J.M., Darbeheshti, M., Baumgardner, D.G., Kok, G.L., Chung, S.H., Schulz, M.,

437        Hendricks, J., Lauer, A., Kärcher, B., Slowik, J.G., Rosenlof, K.H., Thompson, T.L.,

438        Langford, A.O., Loewenstein, M., Aikin, K.C., 2006. Single-particle measurements of

midlatitude black carbon and light-scattering aerosols from the boundary layer to the lower stratosphere. J. Geophys. Res. 111, D16207. http://dx.doi.org/10.1029/2006JD007076.

Schwarz, J.P., Gao, R.S., Spackman, J.R., Watts, L.A., Thomson, D.S., Fahey, D.W., Ryerson, T.B., Peischl, J., Holloway, J.S., Trainer, M., Frost, G.J., Baynard, T., Lack, D.A., de Gouw J.A., Warneke, C., Del Negro, L.A., 2008. Measurement of the mixing state, mass, and optical size of individual black carbon particles in urban and biomass burning emissions. Geophys. Res. Lett. 35, L13810. http://dx.doi.org/10.1029/2008GL033968.

Shiraiwa, M., Kondo, Y., Moteki, N., Takegawa, N., Miyazaki, Y., Blake, D.R., 2007. Evolution of mixing state of black carbon in polluted air from Tokyo. Geophys. Res. Lett. 34, L16803. http://dx.doi.org/10.1029/2007GL029819.

Streets, D.G., Gupta, S., Waldhoff, S.T., Wang, M.Q., Bond, T.C., Bo, Y.Y., 2001. Black carbon emissions in China. Atmos. Environ. 35, 4281–4296.

Sun, Y.L., Wang, Z.F., Fu, P.Q., Jiang, Q., Yang, T., Li, J., Ge, X.L., 2013. The impact of relative humidity on aerosol composition and evolution processes during wintertime in Beijing, China. Atmos. Environ. 77, 927–934. http://dx.doi.org/10.1016/j.atmosenv.2013.06.019.

Sun, Y.L., Jiang, Q., Wang, Z.F., Fu, P.Q., Li, J., Yang, T., Yin, Y., 2014. Investigation of the sources and evolution processes of severe haze pollution in Beijing in January 2013. J. Geophys. Res. 119, 4380–4398. http://dx.doi.org/10.1002/2014JD021641.

Wang, Q.Y., Huang, R.J., Cao, J.J., Han, Y.M., Wang, G.H., Li, G.H., Wang, Y.C., Dai, W.T., Zhang, R.J., Zhou, Y.Q., 2014. Mixing state of black carbon aerosol in a heavily polluted urban area of China: implications for light absorption enhancement. Atmos. Sci. Technol. 48, 689–697. http://dx.doi.org/10.1080/02786826.2014.917758.

Wu, D., 2011. Formation and evolution of haze weather. Environ. Sci. Technol. 34(3), 157–161. (in Chinese)

Xia, X.A., Li, Z.Q., Holben, B., Wang, P.C., Eck, T., Chen, H.B., Cribb, M., Zhao, Y.X., 2007. Aerosol optical properties and radiative effects in the Yangtze Delta region of China. J. Geophys. Res. 112, D22S12. http://dx.doi.org/10.1029/2007JD008859.

Zhang, R.J., Ho, K.F., Cao, J.J., Han, Z.W., Zhang, M.G., Cheng, Y., Lee, S.C., 2009. Organic

carbon and elemental carbon associated with PM10 in Beijing during spring time. J. Hazard. Mater. 172, 970–977. http://dx.doi.org/10.1016/j.jhazmat.2009.07.087.

Zhang, R.J., Jing, J.S., Tao, J., Hsu, S.C., Wang, G.H., Cao, J.J., Lee, C.S.L., Zhu, L., Chen, Z., Zhao, Y., Shen, Z.X., 2013. Chemical characterization and source apportionment of $PM_{2.5}$ in Beijing: seasonal perspective. Atmos. Chem. Phys. 13, 7053–7074. http://dx.doi.org/10.5194/acp-13-7053-2013.

Zhao, X.J., Zhang, X.L., Xu, X.F., Xu, J., Meng, W., Pu, W.W., 2009. Seasonal and diurnal variations of ambient $PM_{2.5}$ concentration in urban and rural environments in Beijing. Atmos. Environ. 43, 2893–2900. http://dx.doi.org/10.1016/j.atmosenv.2009.03.009.

Zhang, Y.L., Huang R.J., Haddad, I.E., Ho, K.F., Cao, J.J., Han, Y., Zotter, P., Bozzetti, C, Daellenbach, K.R., Canonaco, F., Slowik, J.G., Salazar, G, Schwikowski, M., Schnelle-Kreis, J., Abbaszade, G, Zimmermann, R., Baltensperger, U., Prévôt, A.S.H., Szidat, S., 2015. Fossil vs. non-fossil sources of fine carbonaceous aerosols in four Chinese cities during the extreme winter haze episode of 2013. Atmos. Chem. Phys. 15, 1299–1312. http://dx.doi.org/10.5194/acp-15-1299-2015.

Zheng, G.J., Duan, F.K., Su, H., Ma, Y.L., Cheng, Y., Zheng, B., Zhang, Q., Huang, T., Kimoto, T., Chang, D., Pöschl, U., Cheng, Y.F., He, K.B., 2015. Exploring the severe winter haze in Beijing: the impact of synoptic weather, regional transport and heterogeneous reactions. Atmos. Chem. Phys. 15, 2969–2983. http://dx.doi.org/10.5194/acp-15-2969-2015.

Zhuang, B.L., Wang, T.J., Li, S., Liu, J., Talbot, R., Mao, H.T., Yang, X.Q., Fu, C.B., Yin, C.Q., Zhu, J.L., Che, H.Z., Zhang, X.Y., 2014a. Optical properties and radiative forcing of urban aerosols in Nanjing, China. Atmos. Environ. 83, 43–52. http://dx.doi.org/10.1016/j.atmosenv.2013.10.052.

Zhuang, B.L., Wang, T.J., Liu, J., Li, S., Xie, M., Yang, X.Q., Fu, C.B., Sun, J.N., Yin, C.Q., Liao, J.B., Zhu, J.L., Zhang, Y., 2014b. Continuous measurement of black carbon aerosol in urban Nanjing of Yangtze River Delta, China. Atmos. Environ. 89, 415–424. http://dx.doi.org/10.1016/j.atmosenv.2014.02.052.

**Table 1.** Statistical mean value ± standard deviation of BC mass concentration, BC fraction in $PM_{2.5}$, absorption coefficient at 870 nm, and number fraction of thickly-coated BC ($NF_{BC\text{-}thick}$) during the overall campaign (total), non-haze (visibility ≥ 10 km), haze (visibility < 10 km) and heavy haze (visibility < 2 km) episodes.

|  | Total | Non-haze | Haze | Heavy haze |
|---|---|---|---|---|
| BC mass concentration ($\mu g\ m^{-3}$) | 5.5 ± 4.7 | 2.0 ± 1.2 | 7.6 ± 4.8 | 12.5 ± 4.7 |
| BC fraction in $PM_{2.5}$ (%) | 5.7 ± 4.3 | 7.4 ± 6.5 | 5.2 ± 3.2 | 4.0 ± 1.0 |
| Absorption coefficient ($Mm^{-1}$) | 23.6 ± 20.0 | 8.2 ± 5.2 | 33.1 ± 20.2 | 55.9 ± 18.0 |
| $NF_{BC\text{-}thick}$ (%) | 58 ± 20 | 37 ± 9 | 70 ± 14 | 83 ± 3 |
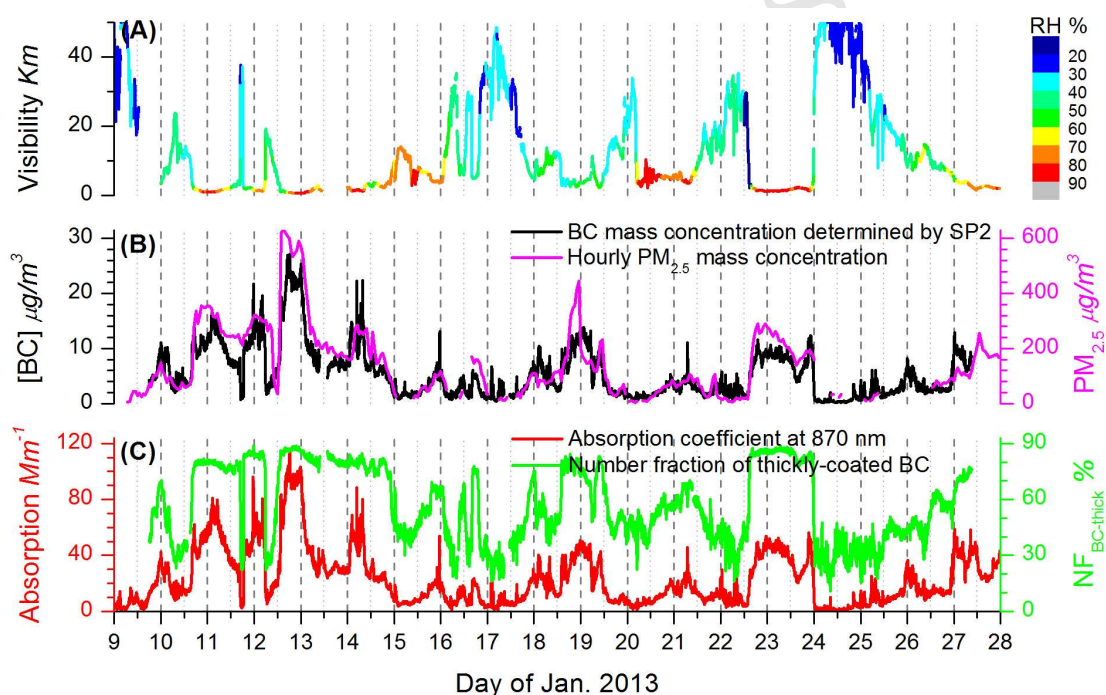


**Figure 1.** Time series of (A) visibility as a function of relative humidity (color scale), (B) $PM_{2.5}$ and BC concentrations, and (C) absorption coefficient at 870 nm and number fraction of thickly-coated BC ($NF_{BC\text{-}thick}$) during the observation period from 9 to 27 January 2013.
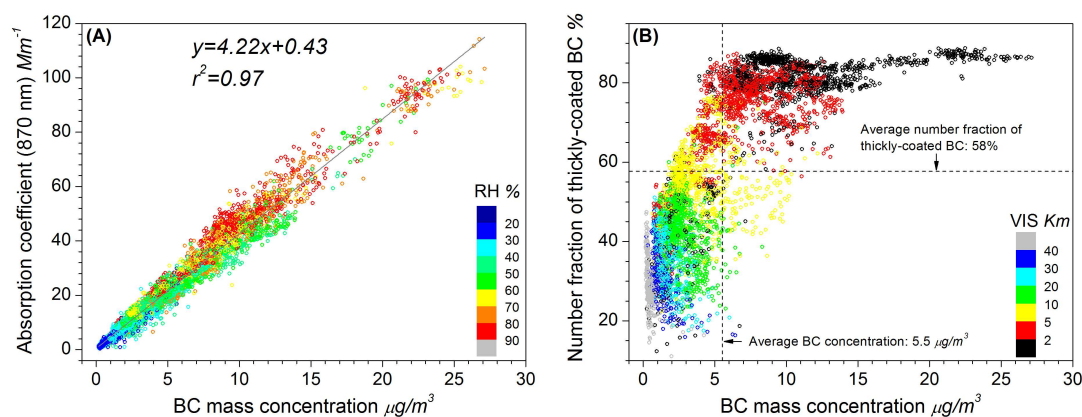
**Figure 2.** Scatter plots of (A) absorption coefficient at 870 nm and (B) number fraction of thickly-coated BC ($NF_{BC-thick}$) against BC concentration, as a function of relative humidity (RH) and visibility range (VIS), respectively (color scales). The vertical and horizontal dashed lines in (B) represent the mean values of BC concentration and $NF_{BC-thick}$, respectively.
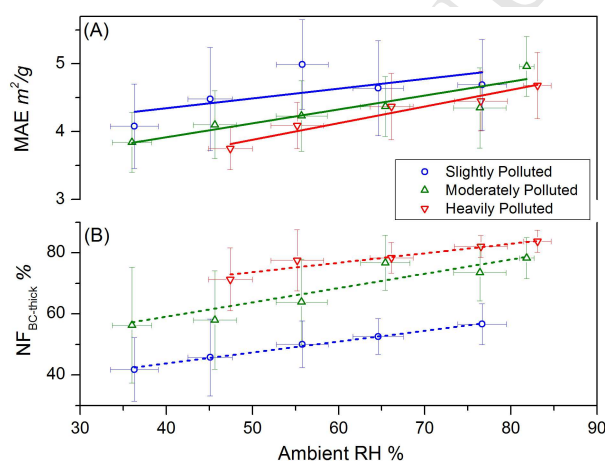


**Figure 3.** Variations of the mean (A) mass absorption efficiency (MAE) of BC and (B) number fraction of thickly-coated BC ($NF_{BC-thick}$) with increasing ambient relative humidity (RH) bins at three BC pollution levels: slightly polluted case with BC concentrations in the range of 25–50th percentile (blue), moderately polluted with BC in the 50–75th percentile (green), and heavily polluted with BC > 75th percentile (red). The corresponding lines are the linear regression of (A) MAE and (B) $NF_{BC-thick}$ against ambient RH. The horizontal and vertical error bars represent one standard deviation. The points included in each RH bin are 347, 375, 105, 116, and 192, from the low to high RH in the slightly polluted case. They are 126, 318, 180, 232, 275 and 198 in the moderately polluted case, and 188, 177, 197, 300 and 349 in the heavily polluted case.

- BC concentrations and mixing states were investigated using a SP2 in urban Beijing.

- BC fraction in $PM_{2.5}$ decreased during haze though its concentrations increased.

- The number fraction of thickly-coated BC increased significantly during haze periods.

- The light absorption of BC was amplified in response to the increasing ambient RH.

1    **Auxiliary material**

2

3    Ambient humidity effect on light absorption amplification of black carbon in

4    Beijing in January 2013

5



6

7
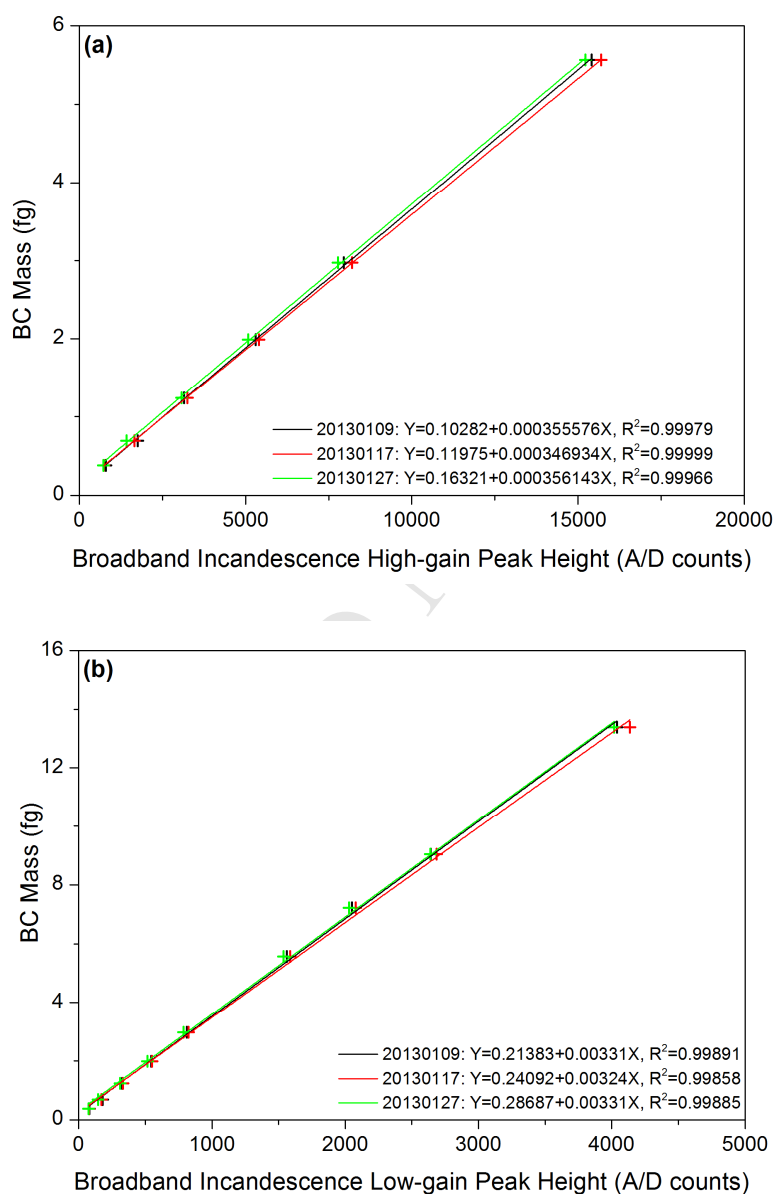
8    **Figure S1**. BC mass calibration curves of the SP2 during the campaign. The

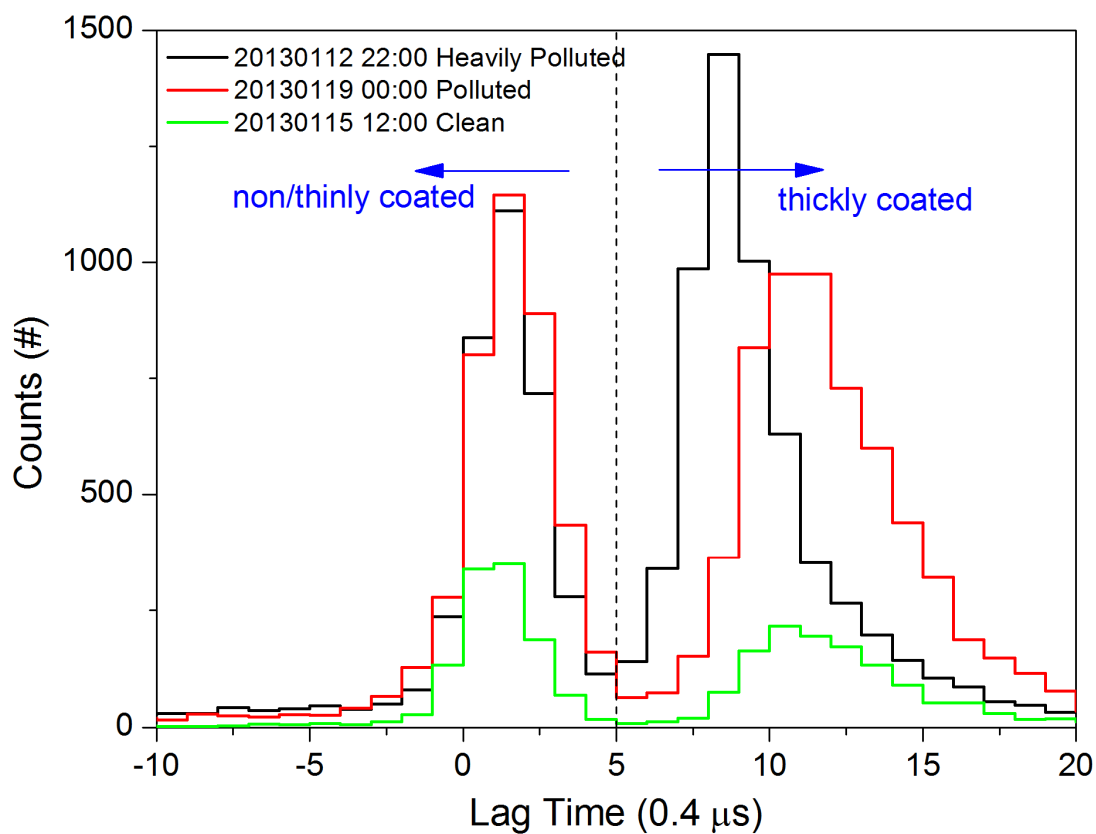9    calibration factors pre-, mid- and post-sampling are very close.

10
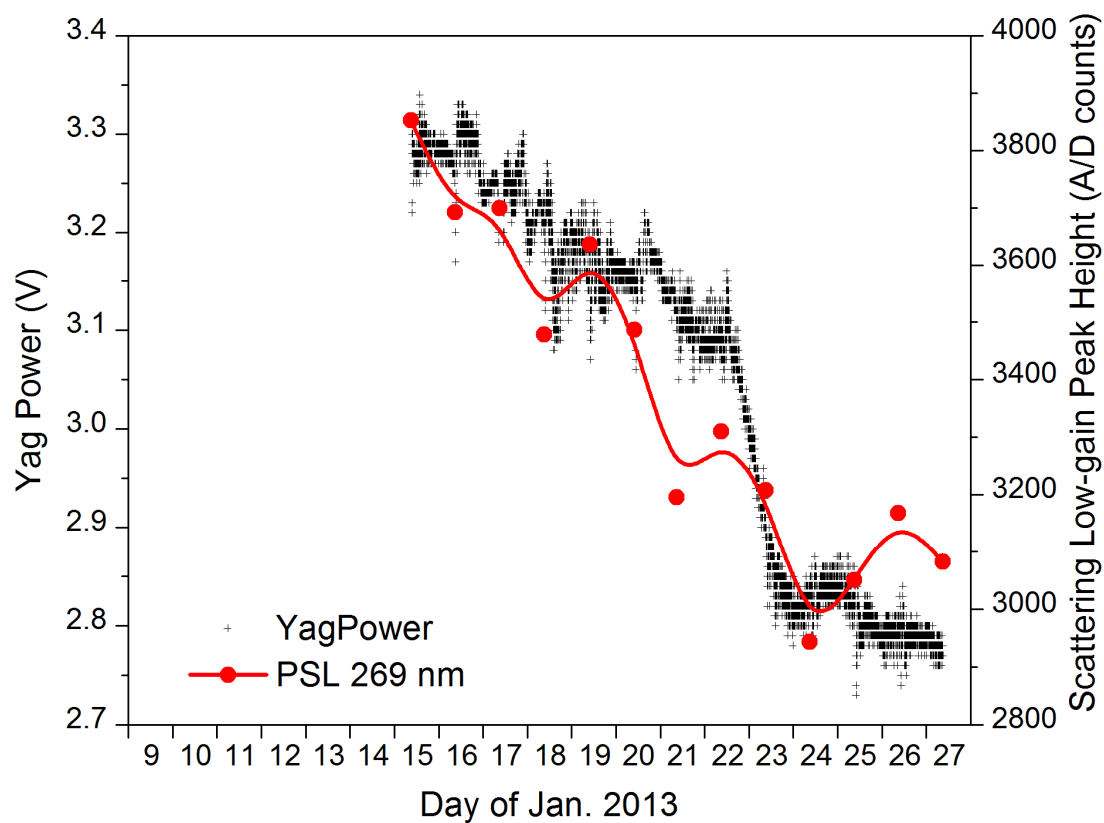
**Figure S2.** Variations of minutely Yag Power recorded by SP2 (black) and the scattering low-gain peak height of PSL with a diameter of 269 nm performed daily during the campaign (red). A decrease by ~30% (from ~3900 to ~3000) in the scattering peak height can be found.

**Figure S3.** Histogram of the lag times between the incandescence and scattering peak locations at three typical pollution levels: heavily polluted (black), polluted (red) and clean (green). A bimodal distribution is found with the minimum at ~2 μs regardless of the pollution level. The BC-containing particles with the lag time greater than 2 μs were considered to be thickly coated. Otherwise, the BC-containing particles were non/thinly coated.
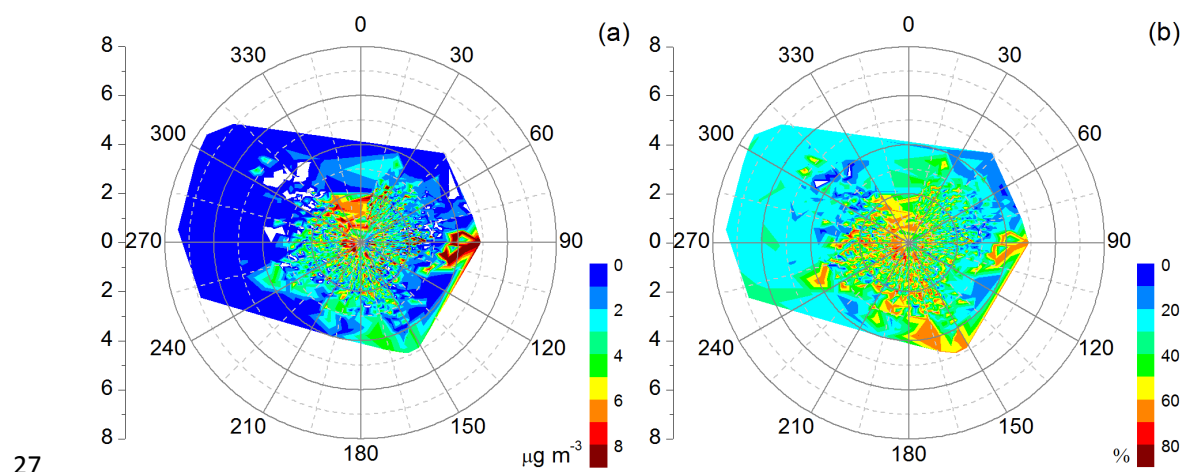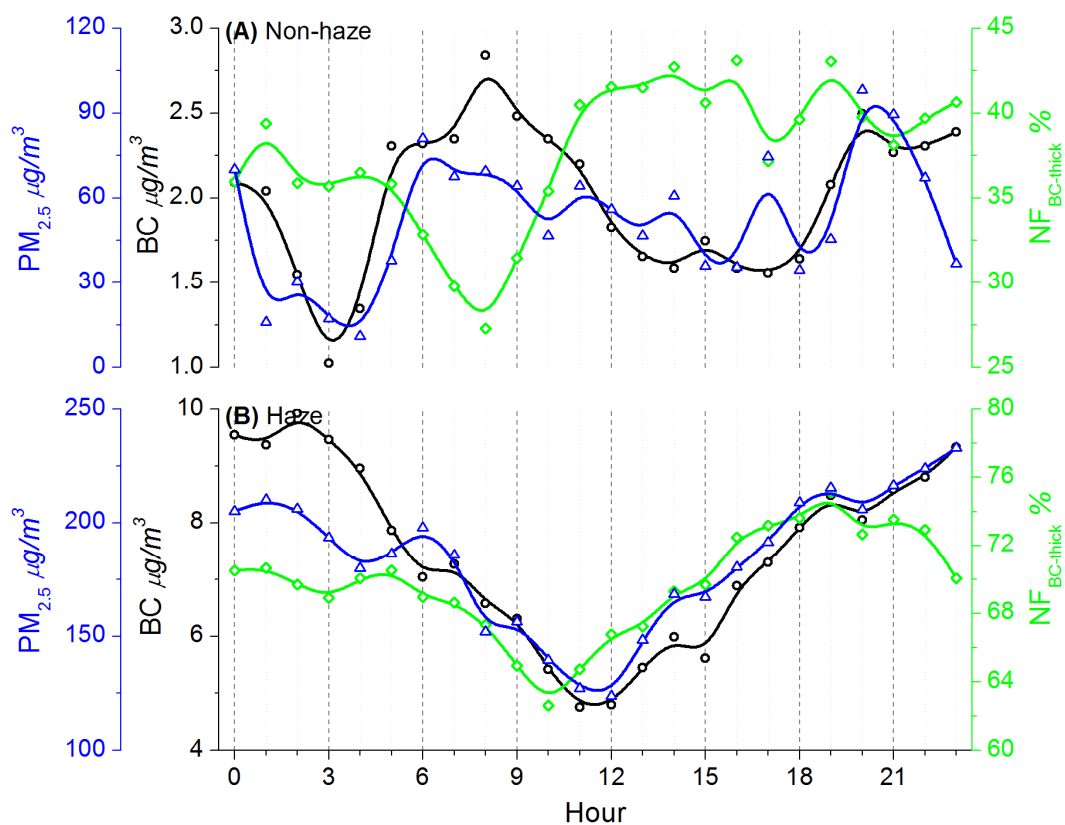
**Figure S4.** Relationship of (a) BC concentrations and (b) the number fractions of the thickly-coated BC particles with winds.

**Figure S5.** Diurnal variations of PM$_{2.5}$ (blue) and BC (black) mass concentrations, and the number fractions of thickly-coated BC-containing particles (NF$_{BC-thick}$, green) during the (A) non-haze and (B) haze periods.

**Table S1.** Previous studies of BC (EC) concentrations in PM$_{2.5}$ in urban Beijing during wintertime.

| BC (EC) ($\mu g\ m^{-3}$) | Observation period | Method | Reference |
|---|---|---|---|
| 11.08 | Winter 1999 | TOR, DRI | He et al. (2001) |
| 2.03 | Jan. 2000 | TOT, NIOSH | Zheng et al. (2005) |
| 15.2 | Dec. 2002 | C/H/N Elemental Analyzer | Dan et al. (2004) |
| 11.0 | Dec. 2002 | C/H/N Elemental Analyzer | Sun et al. (2004) |
| 6.7 | Winter 2005 | TOT, SUNSET | Han et al. (2009) |
| 7.5 | Jan. 2010 | TOR, DRI | Zhang et al. (2013) |
| 5.5 | Jan. 2013 | TOT, EUSAAR_2 | Huang et al. (2014); Zhang et al. (2015) |
| 5.5 | Jan. 2013 | Incandescent, SP2 | This study |

References:

He, K.B., et al., 2001. The characteristics of PM$_{2.5}$ in Beijing, China. Atmos. Environ. 35, 4959–4970.

Zheng, M., Salmon, L.G., Schauer, J.J., Zeng, L.M., Kiang, C.S., Zhang, Y.H., Cass, G.R., 2005. Seasonal trends in PM$_{2.5}$ source contributions in Beijing, China. Atmos. Environ. 39, 3967–3976.

Dan, M., Zhuang, G.S., Li, X.X., Tao, H.R., Zhuang, Y.H., 2004. The characteristics of carbonaceous species and their sources in PM$_{2.5}$ in Beijing. Atmos. Environ. 38, 3443–3452.

Sun, Y.L., et al., 2004. The air-borne particulate pollution in Beijing—concentration, composition, distribution and sources. Atmos. Environ. 38, 5991–6004.

Han, S., et al., 2009. Temporal variations of elemental carbon in Beijing. J. Geophys. Res. 114, D23202.

Huang, R.J., et al., 2014. High secondary aerosol contribution to particulate pollution during haze events in China. Nature 514, 218–222.

Zhang, R.J., et al., 2013. Chemical characterization and source apportionment of PM$_{2.5}$ in Beijing: seasonal perspective. Atmos. Chem. Phys. 13, 7053–7074.

Zhang, Y.L., et al., 2015. Fossil vs. non-fossil sources of fine carbonaceous aerosols in four Chinese cities during the extreme winter haze episode of 2013. Atmos. Chem. Phys. 15, 1299–1312.

59 **Table S2.** Comparison of annual BC emission (Gg) from transportation with total

60 emission for the year of 2009 among Beijing, Shanghai and Guangdong as well as

61 entire China, of which the latter two city/province represent the Yangtze River Delta

62 and Pearl River Delta. Data are taken from the supplementary data of Qin and Xie

63 (2012).

| Megacity / Province / Nation | Transportation | Total |
|---|---|---|
| Beijing | 4.70 | 15.75 |
| Shanghai | 3.76 | 20.49 |
| Guangdong | 21.47 | 43.37 |
| China | 241.19 | 1881.01 |

64

65

66 **Table S3.** Correlation coefficients between BC mass concentration (BC) and the

67 number fractions of thickly-coated BC ($NF_{BC\text{-}thick}$) as well as their mean values in

68 different visibility bins.

| | Non-haze | | | | Haze | | |
|---|---|---|---|---|---|---|---|
| Visibility (km) | ≥40 | 30–40 | 20–30 | 10–20 | 5–10 | 2–5 | <2 |
| Samples | 272 | 255 | 376 | 845 | 870 | 1042 | 813 |
| BC ($\mu g\ m^{-3}$) | 0.5±0.4 | 1.5±0.8 | 1.8±0.8 | 2.7±1.1 | 3.8±2.0 | 7.0±2.9 | 12.5±4.7 |
| $NF_{BC\text{-}thick}$ (%) | 30±6 | 31±7 | 36±7 | 42±7 | 55±9 | 72±11 | 83±3 |
| Spearman-R | -0.48 | -0.42 | -0.50 | -0.23 | 0.21 | 0.48 | 0.05 |

69